A DC Current Flow Controller for Meshed Modular Multilevel Converter Multiterminal HVDC Grids

Na Deng, *Student Member, IEEE*, Puyu Wang, *Student Member, IEEE*, Xiao-Ping Zhang, *Senior Member, IEEE, Member, CSEE*, Guangfu Tang, and Junzheng Cao

***Abstract*—This paper proposes the design of a novel DC current flow controller (CFC) and evaluates the control performance of balancing and regulating the DC branch currents using the DC CFC in a meshed multi-terminal HVDC (MTDC) grid. The DC CFC consists of two identical full bridge DC-DC converters with the capacitors of the two converters being connected in parallel. The scalability of the DC CFC is easily achievable due to the identical bridge converter topology; the cost of this DC CFC is also relatively low due to its simple physical structure and low voltage ratings. The control performance of the DC CFC is tested on a meshed 3-terminal (3-T) HVDC grid, which is based on modular multilevel converters (MMC). The DC branch current control in the meshed MTDC grid is achieved using the proposed control strategy of the DC CFC, and is verified through case studies on the real-time digital simulator (RTDS).**

***Index Terms*—Capacitor voltage control, DC branch current control, DC current flow controller, HVDC transmission, meshed multi-terminal HVDC grid, modular multilevel converter.**

NOMENCLATURE

n-T	n terminal $(n = 1, \cdots, n)$.
T_n	Terminal n $(n = 1, \cdots, n)$.
SM	Submodule.
CFC	Current flow controller.
IGBT	Insulated-gate bipolar transistor.
KCL	Kirchhoff's current law.
LCC	Line commutated converter.
VSC	Voltage sourced converter.
MMC	Modular multilevel converter.
PWM	Pulse-width modulation.
RTDS	Real-time digital simulator.

I. INTRODUCTION

THE HVDC transmission technology is recognized as an advantageous approach for worldwide long-distance bulk-power transmissions [1], [2], with several HVDC applications currently in use for MTDC technologies [3]–[6]. China, at present, has two multi-terminal HVDC grids in operation [5], [6].

Due to its superiority in more efficiently utilizing and integrating renewable energy located in remote areas, MTDC technology has become more attractive in recent years compared to traditional point-to-point HVDCs [7]–[10]. The MTDC system can also be reconfigured into different topologies under faults, particularly after a faulted line is isolated, in order to increase the continuity and reliability of the power supply [10]. Regarding the MTDC technology. Basically, the VSC based technology has more advantages over the LCC based technology [11], [12]. This is because the vector control of the VSC converters, which realizes the independent control of active and reactive power. Hence, for the regulation of power, the VSC based MTDC system is considered more flexible, particularly in instances where the power flow reversal can be easily achieved by reversing the direction of DC currents rather than the reversal of DC voltages. Based on these characteristics, MTDC applications are being increasingly used in HVDC transmission.

Radial interconnections of DC grids, in particular, are being predominantly considered [13], [14] due to their simple configuration and control strategies for regulating power distribution. In a radial topology, there is only one path between two electric nodes, so the power is fully regulated.

Although the radial topology is simple and easy to realize, the meshed topology of DC grids, similar to that of AC grids, is considered as more favorable for real power applications [13], [14]. This is because the meshed topology increases the redundancy of power transmission, which contributes to the enhancement of the reliability of the power system transmission [15], [16].

In a meshed DC grid, the total power exchanged at the converter DC side can be fully controlled; however, the DC current of each branch, depending on the voltage difference of two DC terminals and the resistance of the DC branch, may not be controllable. If there is no additional control strategy to balance the branch currents, the distribution of branch currents will be determined by Kirchhoff's laws.

There is a potential risk that one or more branches of a DC grid may become overloaded, while other branches may be underutilized, since more currents will inherently be delivered to the branch of lower resistance. Therefore, the complexity of the meshed DC grid leads to the potential problems, which

Manuscript received December 1, 2014; revised February 19, 2015; accepted February 25, 2015. Date of publication March 30, 2015; date of current version March 13, 2015. The work was partially supported by UK-China Smart Grid Project ERIFT via UK EPSRC, University of Birmingham Si-Guang Li Scholarship and China Scholarship Council.

N. Deng, P. Wang, and X. P. Zhang are with the School of Electronic Electrical and Systems Engineering, University of Birmingham, Edgbaston, Birmingham B15 2TT, United Kingdom (email: x.p.zhang@ieee.org).

G. Tang and J. Cao are with the State Grid Smart Grid Research Institute, China.

Digital Object Identifier 10.17775/CSEEJPES.2015.00006

are the main concerns of this paper.

There are several control strategies for meshed MTDC grids that have been proposed in the literature. In [17], [18], different droop controllers have been investigated for MTDC grids including meshed topologies. It was found that while the active power of each terminal could be coordinated to a certain extent, the distribution of the DC current on each branch was incapable of being accurately controlled in the meshed grid. A power flow control device for a meshed DC grid has been designed and demonstrated in [13]. In this work, the DC branch current is well controlled by switching on and off the variable resistance of the device. However, the power loss due to switch-in resistance is an undesirable outcome. Reference [19] has presented a power flow control device that provides a detailed system configuration and basic control logic for a meshed DC. However, the control strategy in this device has not been comprehensively analyzed nor a detailed control strategy proposed. A conceptual DC control flow controller (CFC) has been proposed in [14] in which standard full-bridge DC-DC converters with low voltage ratings are used to design the controller. However, only a basic conceptualization of this control device is introduced, and the performance of the branch current control capability is not fully illustrated, while the operating principle and detailed control approach of the device are also not thoroughly investigated.

In this paper, the design of a DC CFC, particularly its detailed control strategy of branch currents, is proposed for a meshed 3-T MMC HVDC grid. The DC CFC is established based on the concept in [14]. The objective of the DC CFC is to control the DC branch currents by transferring the additional power from the overloaded branch to the underutilized branch and to realize this objective with relatively low power losses. The DC branch currents can be regulated at a certain range using the proposed control. The validity of the proposed control strategy of the DC CFC is verified through case studies on the RTDS.

The rest of this paper is organized as follows. Section II presents the meshed 3-T MMC-HVDC system with the system configuration, the control strategy of the MMC at each terminal and an equivalent DC power flow analysis. Section III introduces the meshed MTDC system with the installation of a DC CFC along with the structure of the DC CFC. Section IV explains the proposed control strategy of the DC CFC and features with the proposed control. Case studies and analysis are presented in Section V, followed by conclusions drawn in Section VI.

II. Meshed 3-T MMC-HVDC System

A. System Configuration

A single-line schematic diagram of the investigated meshed 3-T MMC-HVDC system is shown in Fig. 1(a). The three terminals are T_1, T_2, and T_3.

The MTDC system has three (3) identical MMCs. Each MMC, as shown in Fig. 1(b), comprises six (6) converter arms and each arm has n series half-bridge SMs and one series

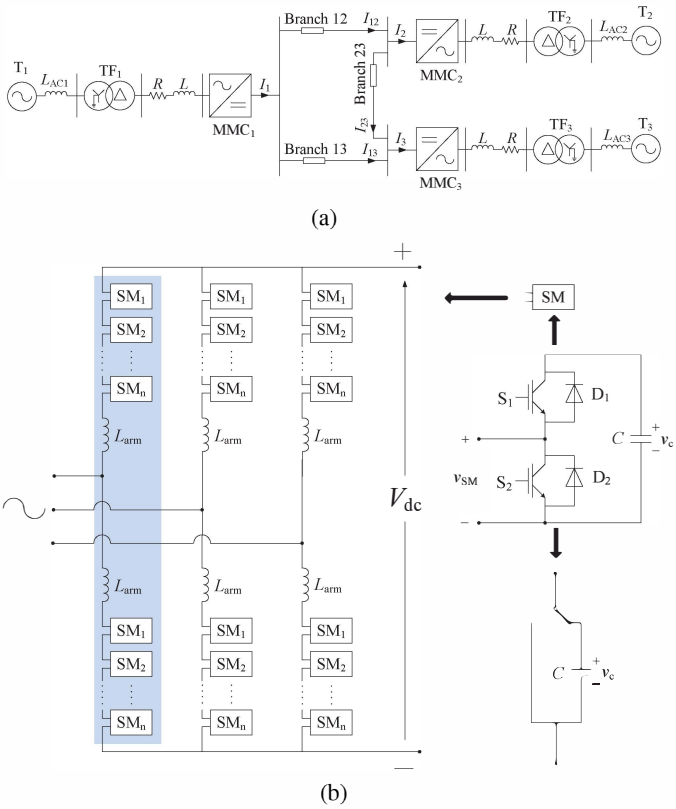

Fig. 1. Configuration of a meshed 3-T MMC-HVDC grid. (a) System configuration. (b) MMC configuration.

inductor L_{arm} per converter arm. Each SM includes an energy storage capacitor C and two switching valves $(\mathrm{S}_1, \mathrm{S}_2)$. Only one switch is switched on during normal operation. Therefore, the output voltage v_{SM} of each SM is either equal to the capacitor voltage v_{c} when the upper switch S_1 is switched on, or equal to zero when the lower switch S_2 is switched on. The MMC modeled in this paper has 6 SMs per converter arm. The MMC DC side is connected to the DC cable, while the MMC AC side is connected to an AC grid at each terminal through a series inductor and resistor as well as a three-phase transformer.

For the DC system, it is a $\pm$50 kV meshed 3-T DC grid. The DC cables are modeled as lumped resistors and the resistance of the DC cable between each terminal, as shown in Table I, is different. For the AC systems of the 3 terminals, their configurations and parameters are identical. Complete system parameters are shown in Table I.

B. Control Strategies of the MMCs

The MMCs are considered as VSC type converters [20]–[22]. The converter level control of the model in this paper applies the classic vector control strategy. Both MMC_1 and MMC_2 apply constant active power control. For the sake of simplification of the system analysis, some assumptions are made: 1) the losses of the converters are neglected; 2) the AC system voltage is constant due to the connection to the AC utility grid; 3) the MMC DC side current is regulated to be constant via the active power control. The total current

TABLE I
PARAMETERS OF THE 3-T MESHED MMC-HVDC SYSTEM IN FIG. 1

Parameter	Value	Parameter	Value
Nominal AC source voltage	138 kV (L-N)	Nominal DC voltage	± 50 kV
L_{AC}	150 mH	MMCs rated capacity	150 MVA
Nominal AC frequency	50 Hz	L_{arm}	3 mH
Transformer voltage ratio	138 kV/30 kV (Y/Δ)	Number of SMs per arm	6
Transformer rating	150 MVA	Submodule capacitor	2,500 μF
Transformer leakage inductance	5%	Branch 12 cable resistance R_{12}	1 Ω
R	0.03 Ω	Branch 13 cable resistance R_{13}	2 Ω
L	1 mH	Branch 23 cable resistance R_{23}	1 Ω

imported from T_1 to the DC grid is kept at 1 kA, while the total current exported from the DC grid to T_2 is kept at 0.4 kA. MMC_3 is controlled to maintain the DC voltage of T_3 at ±50 kV. The reactive power is controlled to be at 0 by all three MMCs.

The capacitor voltage balancing strategy of the MMC employs the conventional sorting method [12]. That is, depending on the arm current direction, the capacitor with a relative lower voltage is charged first, while the capacitor with a relative higher voltage also discharges first.

The DC branch currents I_{12}, I_{13} and I_{23}, which flow via Branch 12, 13, and 23, are not controlled. Thus the distribution of the branch currents largely depends on the cable resistance of each branch. Although most DC cables are constructed of the same material, the lengths of the DC cables between terminals are different and environmental conditions, such as temperature may lead to differences in cable resistance. Therefore, in principle, the cable resistance of each branch is considered to have different values.

If there is no additional strategy to control the DC branch current, the distribution of branch currents, for instance, I_{12}, I_{13} and I_{23}, of the DC grid, are uncontrollable. One or more branches, therefore, may become overloaded, while the other is insufficiently utilized. The principle of electric power transmission is to achieve a maximum utilization of the transmission line/cable within its transfer capability [15]. Therefore, the control of the branch currents is inevitable and necessitates additional controllers.

Since the branch currents of a meshed DC grid are determined by DC cable resistances and DC voltage differences between two terminals, two approaches can be used to control the branch current. One is to change the cable resistance by adding an additional resistor on the DC branch. However, this method significantly increases power losses, which are undesirable. The second method aims at changing the voltage difference between two DC terminals to regulate the branch current. This method is considered a preferable approach since the branch current control is achieved with acceptable low power losses.

C. Equivalent Power Flow Analysis of the Meshed MTDC Grid

The DC nominal voltage of T_3 is regulated at ±50 kV, via the control of MMC_3. Hence, the DC voltage of T_3, V_3, is 100 kV. T_1 imports 1 kA to the DC grid, while T_2 exports 0.4 kA from the DC grid. Thus, the DC currents I_1 and I_2 are 1 kA and 0.4 kA, respectively. The DC buses of MMC_1 and MMC_2 can be simplified and regarded as two ideal DC current sources, while the DC bus of MMC_3 can be considered as an ideal voltage source. The diagram in Fig. 2 presents the simplifications of the DC grid. An equivalent power flow analysis is conducted based on Fig. 2.

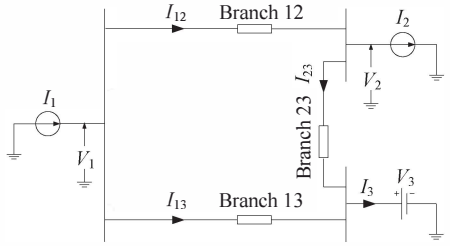

Fig. 2. Configuration of the 3-T MMC-HVDC grid.

Based on Kirchhoff Current Law (KCL), the currents in the meshed MTDC grid have the following relationships:

$$I_1 = I_{12} + I_{13} \tag{1}$$

$$I_3 = I_{13} + I_{23} \tag{2}$$

$$I_1 = I_2 + I_3. \tag{3}$$

According to Ohm's Law, the branch currents in Fig. 2 can be derived as:

$$I_{12} = \frac{V_1 - V_2}{R_{12}} \tag{4}$$

$$I_{13} = \frac{V_1 - V_3}{R_{13}} \tag{5}$$

$$I_{23} = \frac{V_2 - V_3}{R_{23}}. \tag{6}$$

The values of I_1, I_2, and V_3 are determined by the control of MMCs, which means there are six unknown variables in (1)–(6). Therefore, all of their values can be obtained. The expressions of V_1, V_2 and I_3 are derived in (7)–(9).

$$V_1 = V_3 + \frac{I_1 R_{13}(R_{12} + R_{23}) - I_2 R_{23} R_{13}}{R_1 + R_2 + R_3} \tag{7}$$

$$V_2 = V_3 + \frac{I_1 R_{23} R_{13} - I_2 R_{23}(R_{12} + R_{13})}{R_1 + R_2 + R_3} \tag{8}$$

$$I_3 = I_1 - I_2. \tag{9}$$

Referring to the cable parameters listed in Table I and the output DC currents and voltage of the MMCs where I_1 = 1 kA, I_2 = 0.4 kA, V_3 = 100 kV, the voltages and currents of the DC grid are:

DC terminal voltages: V_1 = 100.8 kV, V_2 = 100.2 kV, V_3 = 100 kV;

DC terminal currents: I_1 = 1 kA, I_2 = 0.4 kA, I_3 = 0.6 kA;

DC branch currents: I_{12} = 0.6 kA, I_{13} = 0.4 kA, I_{23} = 0.2 kA.

From the power flow analysis, it is observed that the branch current I_{12} is larger than I_{13}. However, the cables in both branches are made from the same material and thus have the same transfer capability. Hence, Branch 12 is either overloaded or getting closer to its transfer limit, while Branch 13 is insufficiently utilized. Under this condition, a DC CFC with the capability of balancing the branch currents is needed for the meshed MTDC grid to deal with the aforementioned problem, which is discussed in the following sections. The structure of the DC CFC is presented in Section III, the control design is discussed in Section IV and its dynamic performance on balancing and regulating the branch currents is shown in Section V.

III. DC Current Flow Controller

A. Meshed MTDC System with a DC CFC

The DC CFC is equipped on Branch 12 and Branch 13. Fig. 3 shows a single-line schematic diagram of the developed meshed 3-T MMC-HVDC system with the DC CFC being equipped.

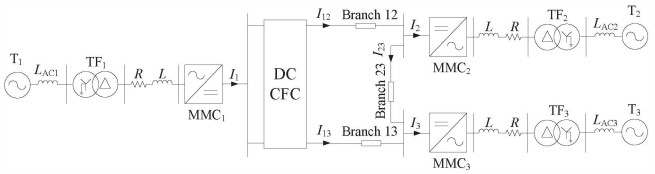

Fig. 3. 3-T MMC-HVDC system with the installation of the DC CFC.

The expected operating condition of the power transmission system is to keep each branch working at its optimal transfer capacity, and this is achievable by the control of the DC CFC, which will be explained in Section IV.

B. Structure of the DC CFC

The detailed structure of the DC CFC installed between Branch 12 and Branch 13 is shown in Fig. 4.

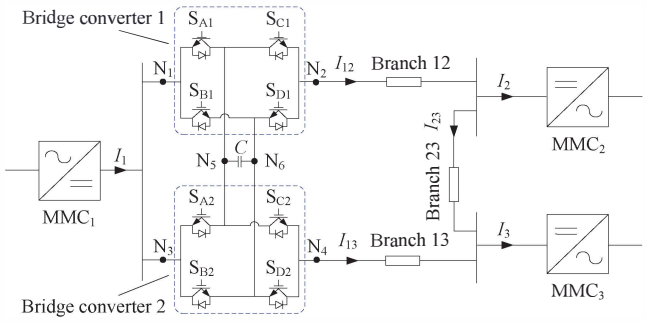

Fig. 4. Structure of the DC CFC.

The DC CFC is composed of two identical full-bridge DC-DC converters. Fig. 5 shows the diagram of an independent full bridge DC-DC converter.

A DC-DC converter has two legs and one energy storage capacitor in the middle. Each leg comprises two IGBTs with their anti-parallel diodes. $\mathrm{S_A}$ and $\mathrm{S_B}$ are on the same leg,

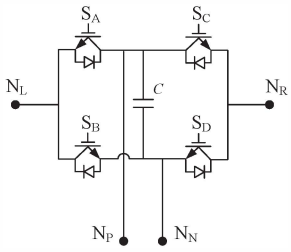

Fig. 5. Full bridge DC-DC converter.

while the other two ($\mathrm{S_C}$ and $\mathrm{S_D}$) compose the other leg. Two switches on the same leg are switched complementary. Consequently, when $\mathrm{S_A}$ is in its off state, $\mathrm{S_B}$ is in the on state, which is the same for $\mathrm{S_C}$ and $\mathrm{S_D}$. This operation manner ensures the two switches on the same leg are never off simultaneously. Under this switching specification, the current through the capacitor is always continuous. The capacitor has three operational states with different switching modes, bypassed, charged, and discharged, as shown in Table II. The capacitor is bypassed when both $\mathrm{S_A}$ and $\mathrm{S_C}$ are on or both $\mathrm{S_B}$ and $\mathrm{S_D}$ are on. The capacitor is charged when both $\mathrm{S_A}$ and $\mathrm{S_D}$ are on, while the capacitor is discharged, when both $\mathrm{S_B}$ and $\mathrm{S_C}$ are on.

TABLE II
Switching Modes with Capacitor Status

Mode	Capacitor State	$\mathrm{S_A}$	$\mathrm{S_B}$	$\mathrm{S_C}$	$\mathrm{S_D}$
1	Bypassed	ON	OFF	ON	OFF
2	Bypassed	OFF	ON	OFF	ON
3	Charged	ON	OFF	OFF	ON
4	Discharged	OFF	ON	ON	OFF

The DC CFC is composed of the connection of two DC-DC converters. The interconnection points are the positive and negative side $(\mathrm{N_P}, \mathrm{N_N})$ of the capacitor, respectively, as shown in Fig. 5.

IV. Control Strategy of the DC CFC

The objective of using the DC CFC is to realize the control of the branch currents in the meshed 3-T MMC-HVDC grid. The equivalent power flow analysis of the meshed MTDC grid derived in Section II-C indicates that it is necessary to balance the current distribution of Branch 12 and Branch 13 through the control of the DC CFC. This is achieved by transferring additional power from Branch 12 to Branch 13 via the energy storage capacitor.

Under steady-state condition, the imported and exported power of the interconnected capacitor should be equal. In order to realize the control of the branch currents, not only the branch current I_{12} needs to be regulated, but the voltage of the interconnected capacitor V_{c} needs to be controlled as well. This is because a stable capacitor voltage indicates that the power exchange of the capacitor is balanced. In addition, the voltage of a capacitor represents the energy stored in the capacitor. The energy of a capacitor can be approximately represented by its average voltage:

$$W_{\mathrm{c}} = \frac{1}{2} C V_{\mathrm{c}}^2. \tag{10}$$

V_c is the average voltage stored in the capacitor. The power imported and exported of a capacitor is depicted in Fig. 6.

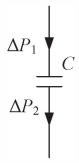

Fig. 6. Power imported and exported of a capacitor.

Under steady-state conditions, the power exchange of the interconnected capacitor is balanced, so

$$\Delta P_1 = \Delta P_2. \tag{11}$$

That means the power imported to the capacitor equals to the power exported from the capacitor, so the power of the capacitor P_c is zero.

As power is defined as the derivative of work, we have

$$\frac{dW_c}{dt} = P_c = 0. \tag{12}$$

According to (10) and (12), the capacitor voltage should be controlled to maintain a certain value under steady-state conditions based on the operating condition of the DC CFC.

The basic control strategy of the DC CFC is similar to that of a point-to-point VSC-HVDC system in which DC voltage control is employed by one converter station at one terminal to maintain the voltage of the DC grid, while active power flow control is applied by the other converter station to determine the amount of power and its direction. Therefore, one terminal is operated as a slack DC terminal, the active power of which can be either imported or exported depending on the operating condition of the other terminal.

For the DC CFC modeled in this paper, the DC-DC converter on Branch 12 is assigned to control branch current I_{12}. When I_{12} is controlled, the current on Branch 13, I_{13}, is determined simultaneously. This is because the total current of Branch 12 and Branch 13, I_1, is regulated at 1 kA by the control of MMC_1. The other DC-DC converter on Branch 13 is responsible for regulating the voltage of capacitor C_2. Since two capacitors of the DC-DC converters are connected in parallel, they always have the same voltage value.

From the structure of the DC CFC, as shown in Fig. 4, $\mathrm{S_{A1}}$ and $\mathrm{S_{A2}}$ are connected in parallel, and this is same for $\mathrm{S_{B1}}$ and $\mathrm{S_{B2}}$. Thus, to maintain the voltage of the capacitors, the operation of $\mathrm{S_{A1}}$ and $\mathrm{S_{A2}}$ must be synchronous. Meanwhile, the operation of $\mathrm{S_{B1}}$ and $\mathrm{S_{B2}}$ are also synchronous and should be complementary with $\mathrm{S_{A1}}$ and $\mathrm{S_{A2}}$. In fact, in the existence of $\mathrm{S_{A1}}$ and $\mathrm{S_{B1}}$ of the DC-DC converter on Branch 12, $\mathrm{S_{A2}}$ and $\mathrm{S_{B2}}$ of the other DC-DC converter are not necessarily needed. However, in order to maintain a higher redundancy of the meshed DC grid, four switches on both DC-DC converters are retained. In addition, $\mathrm{S_{A1}}$ and $\mathrm{S_{A2}}$ are both named as $\mathrm{S_A}$ with a same controlled gating signal ($\mathrm{G_A}$) while $\mathrm{S_{B1}}$ and $\mathrm{S_{B2}}$ are both named as $\mathrm{S_B}$ with a complementary gating signal ($\mathrm{G_B}$).

According to Table II, the capacitor of the DC-DC converter shown in Fig. 5 is charged with switching mode 3 and is discharged with mode 4. The duty ratio of each switch of the full-bridge DC-DC converter is $\mathrm{D_{S}}_J$ ($J = \mathrm{A, B, C, D}$) and the generated gating signal is $\mathrm{G_{S}}_J$. The gating signal is produced through the PWM by comparing the controlled signal with a sawtooth wave. Two general operating states within two switching cycles are depicted in Fig. 7.

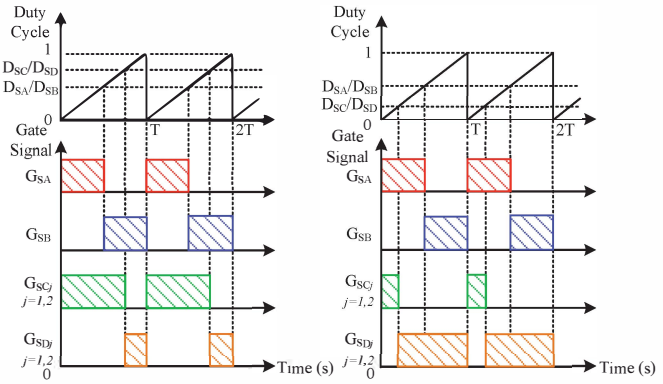

Fig. 7. Gate signal generation of each switch.

In Fig. 4, Branch 12 needs to transfer its power to Branch 13 by charging the interconnected capacitor, while Branch 13 needs to obtain the excess power from Branch 12 by discharging the interconnected capacitor. Due to the characteristics of complementary switching, only one switch on one leg needs to be controlled. For the DC CFC modeled in this paper, $\mathrm{S_A}$, $\mathrm{S_{C1}}$ and $\mathrm{S_{C2}}$ are controlled. In order to simplify the following analysis, the duty ratios of $\mathrm{S_A}$ and $\mathrm{S_B}$, $\mathrm{D_{SA}}$, and $\mathrm{D_{SB}}$, are both fixed at 0.5. The branch current control and the capacitor voltage control will thus be achieved by controlling the switches $\mathrm{S_{C1}}$ and $\mathrm{S_{C2}}$.

A. Branch Current Control

The branch current control is implemented through regulating the difference of the duty ratio between $\mathrm{S_A}$ and $\mathrm{S_{C1}}$. As the switching performance is shown in Fig. 7, when the duty ratio difference $\mathrm{D_{SA}} - \mathrm{D_{SC1}}$ is positive, the interconnected capacitor is charged and I_{12} becomes smaller. The measurement of branch current 12 ($I_{12\mathrm{meas}}$) is tracking its reference value ($I_{12\mathrm{ref}}$) by the application of a ***PI*** controller. Fig. 8 illustrates the control approach.

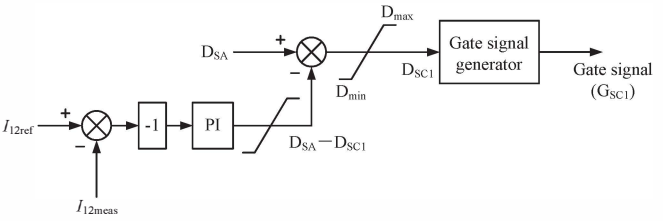

Fig. 8. Branch current control system.

In Fig. 8, a larger (smaller) $I_{12\mathrm{meas}}$ than $I_{12\mathrm{ref}}$ leads to a decrease (increase) in the generated duty cycle of $\mathrm{S_{C1}}$. Thus, the interconnected capacitor will be charged (discharged) more with switching mode 3 and $I_{12\mathrm{meas}}$ will be reduced (increased) to track $I_{12\mathrm{ref}}$.

B. Capacitor Voltage Control

The control of the capacitor voltage is similar to that of the branch current, via a *PI* controller. The control approach is illustrated in Fig. 9. A positive (negative) tracking error signifies the measured capacitor voltage is smaller (larger) than its reference voltage and will result in a decrease (increase) in the generated duty ratio of S_{C2}. Thus, the interconnected capacitor will be charged (discharged) with switching mode 3 and $V_{\rm cmeas}$ will be increased (decreased) to track the control reference.

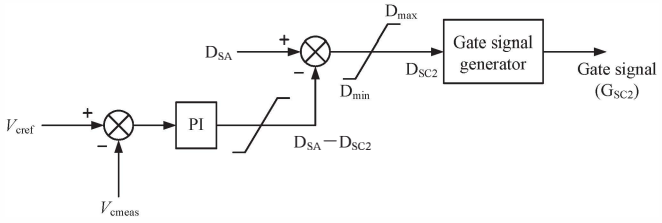

Fig. 9. Capacitor voltage control.

C. Start-up Process of the DC CFC

Initially, the DC CFC is in standby mode, i.e., the interconnected capacitor is bypassed, so the capacitor voltage is zero and the branch currents are not controlled. $I_{\rm meas}$ (0.6 kA) is larger than the reference value (0.5 kA). When the DC CFC is started to control the branch currents, the duty ratios of S_{C1} and S_{C2} generated are both decreased, leading to the charging of the interconnected capacitor. Hence, the voltage of the interconnected capacitor will be fast charged to the reference value and $I_{\rm meas}$ will decrease during the charging process. A new steady-state condition will be achieved when the power exchanged between the capacitor is balanced, the voltage of the capacitor is well maintained and the branch current is regulated to the reference value.

D. Features of the DC CFC

The DC CFC with the proposed control has two main features: 1) branch current balancing capability; 2) branch current regulating capability.

1) Branch Current Balancing Capability: In the meshed MTDC grid, an equal distribution of the branch currents at one terminal junction is expected when the transmission capabilities of both cables are the same. However, different lengths of branches and the impact of the environmental conditions lead to different cable resistance, so the natural distribution of branch currents in a meshed grid is usually unbalanced. The DC CFC with the proposed control in the meshed MTDC grid has the ability to regulate the DC branch current to achieve equal distribution of the branch currents.

2) Branch Current Regulating Capability: In some meshed MTDC applications, the transmission capabilities of DC cables are different; it is expected that the power transfer on one branch can be operated over another branch. Hence, instead of the equal DC branch current distribution, a proportional distribution of the branch currents at one terminal junction is desired to facilitate the optimal operating state of each branch. The DC CFC with the proposed control is capable of regulating the DC branch currents within a certain range. The balancing and regulating capabilities of the branch current of the DC CFC will be verified through case studies in the next section.

V. Simulation Systems and Case Studies

A. Simulation Systems

The simulation system is the meshed 3-T MMC-HVDC system, as shown in Fig. 3, using the parameters provided in Table I. The structure of the DC CFC used in the simulation is the same as shown in Fig. 4. The interconnect capacitor C is 30 μF, and the rated voltage of the IGBTs of the DC CFC is 10 kV. The control strategies of the MMCs and the control strategy of the DC CFC are explained in Section II-B and Section IV, respectively.

B. Case Studies

1) Branch Current Balancing Capability: Initially, the DC CFC is in standby mode. The DC CFC starts to balance the branch currents at 1 s. $I_{12\rm ref}$ is set to 0.5 kA, and $V_{\rm cref}$ is set to 1 kV.

Fig. 10(a) shows the MMC DC side current at each terminal. I_1 = 1 kA, I_2 = 0.4 kA, and I_3 = 0.6 kA. Only a small ripple is observed at 1 s when the DC CFC is operating to balance the branch currents. Fig. 10(b) shows three branch currents with natural distributions of each terminal before 1 s. It is observed that by bypassing the interconnected capacitor at the initial stage, the DC CFC does not perform the balancing function of the branch currents and the system is operating just as the system shown in Fig. 1(a) without the DC CFC in which branch current I_{12} = 0.6 kA, I_{13} = 0.4 kA, and I_{23} = 0.2 kA. At 1 s, both I_{12} and I_{13} reach 0.5 kA within 0.5 s. The DC voltage of the interconnected capacitor is shown in Fig. 10(c). The capacitor voltage $V_{\rm c}$ is zero when the capacitor is bypassed. At 1 s, the power is transferred via the capacitor, and $V_{\rm c}$ is charged to 1 kV within 0.1 s. The DC side voltage of $\rm MMC_3$ is shown in Fig. 10(d). V_3 has a small voltage drop when the balancing control of the branch current is applied, but it resumes 100 kV within 1 s. The overall results indicate the effectiveness of the DC CFC in balancing the branch currents.

2) Branch Current Regulating Capability: Initially, the DC CFC is with the mode of balancing the branch current. At 1s, the logic of regulating the branch currents performs its role where $I_{12\rm ref}$ is set to 0.7 kA, and $V_{\rm cref}$ is still set to 1 kV.

Fig. 11(a) demonstrates that the currents at three DC terminals are well stabilized at their reference values after applying the branch current regulating control of the DC CFC. Fig. 11(b) shows that at 1 s, I_{12} is tracking its reference signal to 0.7 kA, while I_{13} is decreasing to 0.3 kA and I_{23} is increasing to 0.3 kA; both branch currents reach the new steady-state condition within 1 s. The voltage of the interconnected capacitor is maintained at 1 kV with a small voltage dip as shown in Fig. 11(c). The DC voltage of $\rm T_3$ and V_3, has a slight decrease after 1 s, but it returns to the reference voltage within 1 s, as shown in Fig. 11(d). The performance of

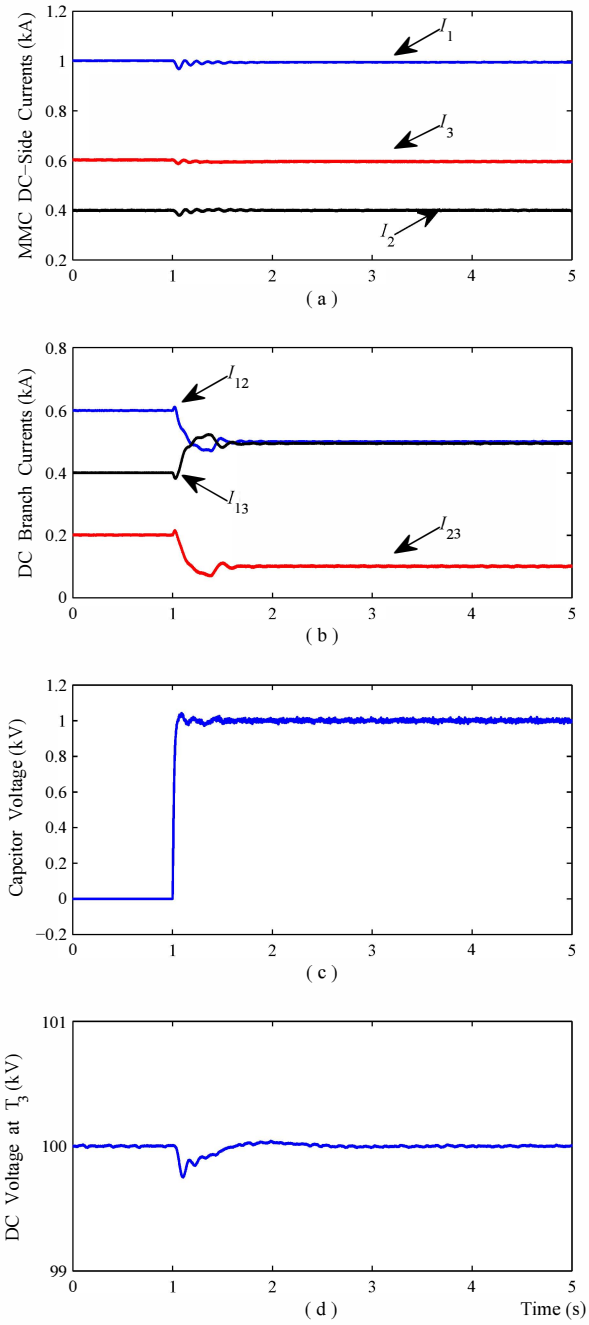

Fig. 10. System performance with branch current balancing control of the DC CFC. (a) I_1, I_2, I_3 are the DC currents of $\mathrm{T}_1, \mathrm{T}_2$, and T_3, respectively. (b) I_{12}, I_{13}, and I_{23} are the DC currents of Branch 12, 13, and 23, respectively (c) Voltage of the interconnected capacitor (d) DC voltage at T_3.

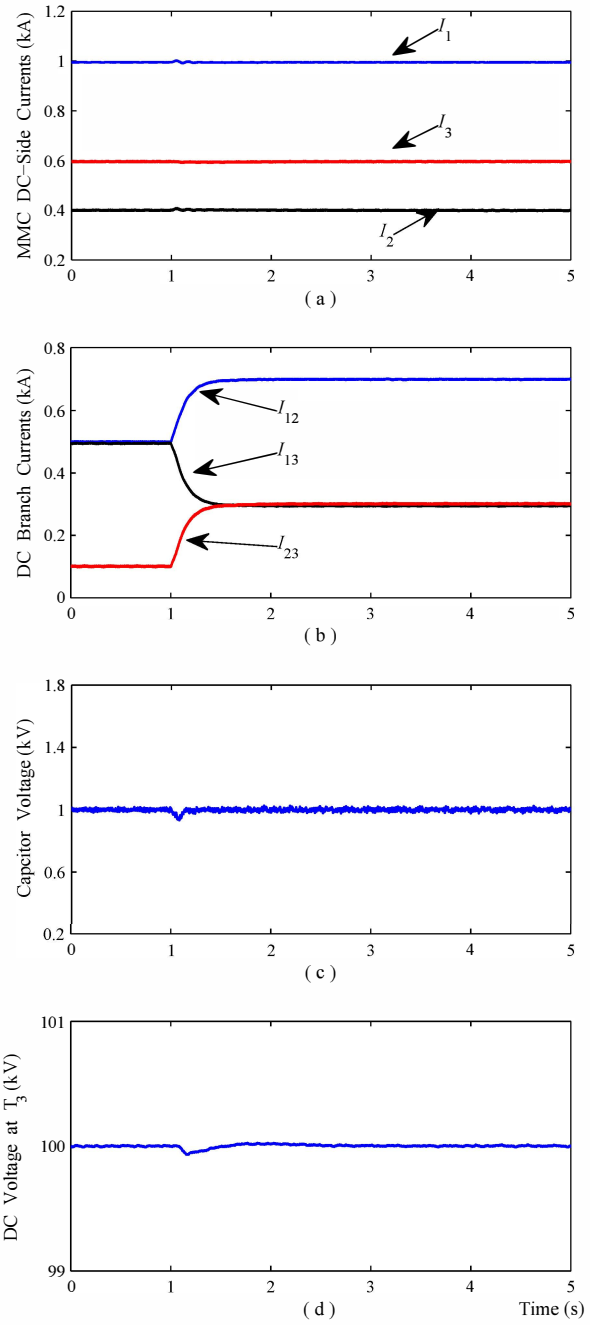

Fig. 11. System performance with branch current regulating control of the DC CFC. (a) I_1, I_2, I_3 are the DC currents of $\mathrm{T}_1, \mathrm{T}_2$, and T_3, respectively. (b) I_{12}, I_{13}, and I_{23} are the DC currents of Branch 12, 13, and 23, respectively (c) Voltage of the interconnected capacitor (d) DC voltage at T_3.

the branch currents and capacitor voltage validate the branch current regulating control of the DC CFC.

The simulation results shown in Fig. 10 and Fig. 11 illustrate that the branch currents can not only be equally distributed, but also be regulated within a certain range as well.

VI. Conclusion

This paper has proposed the design of a DC CFC, particularly its detailed control strategy, in order to control the branch currents in a meshed 3-T MMC-HVDC grid. An equivalent power flow analysis of the 3-T meshed grid under the steady-state condition has been derived. It has been found that for the system without DC CFC, the branch currents are uncontrollable and one or more branches may become either overloaded or underutilized. The structure of the DC CFC has been presented with its operation theorem being proposed. The DC CFC has features of branch current balancing and regulating capability with the proposed control, which has been validated through case studies on the RTDS. These features allow the branches to avoid overloading and

to operate under optimal condition. This DC CFC with the proposed control can be regarded as an effective model for the branch current control in a meshed DC grid.

REFERENCES

[1] M. P. Bahrman and B. K. Johnson, "The ABCs of HVDC transmission technologies," *IEEE Power and Energy Magazine*, vol. 5, no. 2, pp. 32–44, 2007.

[2] N. Flourentzou, V. G. Agelidis, and G. D. Demetriades, "VSC-based HVDC power transmission systems: An overview," *IEEE Transactions on Power Electronics*, vol. 24, no. 3, pp. 592–602, 2009.

[3] T. M. Haileselassie and K. Uhlen, "Power system security in a meshed North Sea HVDC grid," *Proceedings of the IEEE*, vol. 101, no. 4, pp. 978–990, 2013.

[4] D. Van Hertem and M. Ghandhari, "Multi-terminal VSC HVDC for the European supergrid: Obstacles," *Renewable and Sustainable Energy Reviews*, vol. 14, no. 9, pp. 3156–3163, 2010.

[5] G. Bathurst and P. Bordignan, "Delivery of the Nanao multiterminal VSC-HVDC system," presented at *IET 11th International Conference on AC DC Power Transmission*, Feb. 2015.

[6] X. J. Guo, S. S. Zhao, Y. H. Wang, G. Q. Bu, and Q. Guo, "Discussion on cascade-connected multiterminal UHVDC system and its application," in *IEEE Power and Energy Society General Meeting*, 2012, pp. 1–5.

[7] X. P. Zhang, "Multiterminal voltage-sourced converter-based HVDC models for power flow analysis," *IEEE Transactions on Power Systems*, vol. 19, no. 4, pp. 1877–1884, 2004.

[8] X. Chen, H. Sun, J. Wen, W. J. Lee, X. Yuan, N. Li, and L. Yao, "Integrating wind farm to the grid using hybrid multiterminal HVDC technology," *IEEE Transactions on Industry Applications*, vol. 47, no. 2, pp. 965–972, 2011.

[9] O. Gomis-Bellmunt, A. Egea-Alvarez, A. Junyent-Ferré, J. Liang, J. Ekanayake, and N. Jenkins, "Multiterminal HVDC-VSC for offshore wind power integration," in *IEEE Power and Energy Society General Meeting*, 2011, pp. 1–6.

[10] P. Wang, X. P. Zhang, P. F. Coventry, and Z. Li, "Control and protection strategy for MMC MTDC system under converter-side AC fault during converter blocking failure," *Journal of Modern Power Systems and Clean Energy*, vol. 2, no. 3, pp. 272–281, 2014.

[11] M. Davies, M. Dommaschk, J. Dorn, J. Lang, D. Retzmann, and D. Soerangr, "HVDC plus—basics and principle of operation," in *Special Edition for Cigré Exposition*, 2008.

[12] M. Saeedifard and R. Iravani, "Dynamic performance of a modular multilevel back-to-back HVDC system," *IEEE Transactions on Power Delivery*, vol. 25, no. 4, pp. 2903–2912, 2010.

[13] Q. Mu, J. Liang, Y. Li, and X. Zhou, "Power flow control devices in DC grids," in *IEEE Power and Energy Society General Meeting*, 2012, pp. 1–7.

[14] C. Barker and R. Whitehouse, "A current flow controller for use in HVDC grids," in *10th IET International Conference on AC and DC Power Transmission (ACDC)*, 2012, pp. 1–5.

[15] X. P. Zhang, C. Rehtanz, and B. Pal, *Flexible AC Transmission Systems: Modelling and Control*. Berlin: Springer, 2012.

[16] F. Kreikebaum, D. Das, J. Hernandez, and D. Divan, "Ubiquitous power flow control in meshed grids," in *IEEE Energy Conversion Congress and Exposition (ECCE)*, 2009, pp. 3907–3914.

[17] T. M. Haileselassie and K. Uhlen, "Impact of DC line voltage drops on power flow of MTDC using droop control," *IEEE Transactions on Power Systems*, vol. 27, no. 3, pp. 1441–1449, 2012.

[18] N. R. Chaudhuri and B. Chaudhuri, "Adaptive droop control for effective power sharing in multi-terminal DC (MTDC) grids," *IEEE Transactions on Power Systems*, vol. 28, no. 1, pp. 21–29, 2013.

[19] L. E. Juhlin, "Power flow control in a meshed HVDC power transmission network," Sep. 30, 2014, US Patent 8,847,430.

[20] A. Lesnicar and R. Marquardt, "An innovative modular multilevel converter topology suitable for a wide power range," in *IEEE Power Tech Conference Proceedings*, vol. 3, 2003, pp. 1–6.

[21] K. Li and C. Zhao, "New technologies of modular multilevel converter for VSC-HVDC application," in *Asia-Pacific Power and Energy Engineering Conference (APPEEC)*, 2010, pp. 1–4.

[22] H. Saad, J. Peralta, S. Dennetiere, J. Mahseredjian, J. Jatskevich, J. Martinez, A. Davoudi, M. Saeedifard, V. Sood, X. Wang *et al.*, "Dynamic averaged and simplified models for MMC-based HVDC transmission systems," *IEEE Transactions on Power Delivery*, vol. 28, no. 3, pp. 1723–1730, 2013.

Na Deng (S'13) received the BEng degree from Huazhong University of Science and Technology (HUST), China in 2011. Since 2011, she has been pursuing the PhD degree at the University of Birmingham, UK. Her research interests are the applications of DC/DC, AC/DC converters in HVDC systems and microgrids.

Puyu Wang (S'13) received the B.Eng. degree from the University of Birmingham, UK and Huazhong University of Science and Technology (HUST), China, respectively, in 2011, both in electrical engineering. He is now pursuing the PhD degree at the University of Birmingham, UK. He has been a research fellow in electrical power systems at the same university since 2013. His research interest includes HVDC technology, power electronics applications in power systems, DC-DC converters and integration of renewable energy into power grids.

Xiao-Ping Zhang (M'95, SM'06) received the B.Eng., MSc and Ph.D. degrees in electrical engineering from Southeast University, China in 1988, 1990, 1993, respectively. He is currently Professor in Electrical Power Systems and Director of Smart Grid of Birmingham Energy Institute at the University of Birmingham, UK. Before joining the University of Birmingham, he was an Associate Professor in the School of Engineering at the University of Warwick, UK. From 1998 to 1999, he was visiting UMIST. From 1999 to 2000, he was an Alexander-von-Humboldt Research Fellow with the University of Dortmund, Germany. He worked at China State Grid EPRI on EMS/DMS advanced application software research and development between 1993 and 1998. He is co-author of the monograph *Flexible AC Transmission Systems: Modeling and Control* (New York: Springer, 2006 and 2012). Prof Zhang is an Editor of the IEEE Transactions on Smart Grid. Internationally, Professor Zhang pioneered the concept of 'Global Power & Energy Internet' and 'Energy Union'.

Guangfu Tang received the B.Eng. degree in electrical engineering from Xi'an Jiao Tong University, Shanxi, P.R. China, in 1990. He earned his M.Eng. degree and Ph.D. degree in electrical engineering from the Institute of Plasma Physics and The Chinese Academy of Sciences (ASIPP) in 1993 and 1996, respectively. From 1996 to1998, he held a post-doctoral position with China Electric Power Research Institute (CEPRI), Beijing, P. R. China, and he was the vice director of China Energy Conservation Center. In 1998, he joined the CEPRI, where he led the Thyristor Controlled Series Compensator Group from 1998 to 1999, and the Static Var Compensator from 2000 to 2001. Since 2002, he has been a professorial senior engineer of CEPRI. During the past 16 years, his research elds include the fault current limiter, the converter valve of high voltage or ultra high voltage in DC transmission system, and the voltage-source converter-high voltage dc (VSC-HVDC) transmission systems. Now, he is Vice President of State Grid Smart Grid Research Institute (SGSGRI). He has published more than 110 papers, and won 70 patents in his research fields. Dr. Tang is the recipient of the 2006 Second Award, and the 2008 First Award of the National Science and Technology Progress of P. R. China, respectively. He has obtained 6 Provincial Scientific and Technological Progress Awards. He was the convenor of 48 working groups in the International Council on Large Electric Systems in 2007. Now, he sits on a committee of the IEEE/PES Narain Hingorani FACTS and Custom Power Award Committee.

Junzheng Cao received his M.Sc. degree in 1985 from Xi'an Jiaotong University in China and his Ph.D. degree in 1997 from South Bank University, UK. He is currently a professorate senior engineer of State Grid Smart Grid Research Institute (SGSGRI), and a chief engineer at C-EPRI Electrical Engineering Co. Ltd., both being sub-organizations of the State Grid Corporation of China (SGCC). He was cited as China's National Distinguished Expert of "1000-Elit Program" in 2010, and was a guest professor of Xian Jiaotong University in 2012. Prior to returning to China in 2010, he served as a principal engineer and an HVDC expert at AREVA/ALSTOM T&D. Since his return to China in 2010, he has authored/co-authored over 30 HVDC-related technical papers, 17 patents, and a book titled, *China Electric Power Encyclopedia*. Dr. Cao is a member of IEEE, IET, and Cigre, and a member of several working groups including IEC TC22/22F/MT10, IEC TC22/22F/WG26, National Technical Committee 60 on Power Electronics of Standardization Administration of China (SAC/TC60/SC2), and has recently been accepted as an expert contributing member of the Cigre working group B4-62. He is a paper reviewer of *IEEE Trans on Smart Grid* and *IET Trans on Instr. & Meas.* His research interests are in the development and engineering of power electronics for FACTS, HVDC, and future DC grid applications.